

# FREE VIBRATIONS OF CYLINDRICAL PANELS WITH CUTOUTS BY A SINGLE-DOMAIN RITZ FORMULATION

A. Milazzo<sup>1</sup> & M. Lo Cascio<sup>1</sup>

<sup>1</sup>University of Palermo, Department of Engineering, V.le delle Scienze, Bld. 8, 90128, Palermo, Italy

#### **Abstract**

A novel single-domain Ritz approach is proposed for the free vibration analysis of laminated cylindrical panels with cutouts. The panel structural model is based on the first order shear deformation theory and the problem primary variable, namely the midplane translations and the section rotations, are approximated by a set of trial functions built as the tensor product of one-dimensional orthogonal Legendre polynomials. The problem governing equations in terms of the primary variables unknown Ritz coefficients are determined by the stationarity condition of the total energy potential obtaining the algebraic resolving system. The matrices of the resolving system are computed using a special integration technique that, based on the implicit description of the cutout via a suitably-defined level set function, allows for an accurate evaluation of the involved integrals over the panel domain. To show the potential of the method, validation results and studies are presented, highlighting the features of the approach and its capability in dealing with general configurations with respect edge constraints, layups and cutout shape and position.

**Keywords:** Ritz method, composite shells, free-vibration analysis

#### 1. Introduction

Laminated cylindrical panels have great importance in aerospace applications due to their structural effectiveness and potential for significant weight savings and enhanced structural performance resulting from innovative design and optimisation strategies. When dynamic loads are applied to these structural components, they can induce larger strain and stress fields than predicted by static analyses, especially when the structure's natural frequencies are excited [1]. Therefore, it is essential to investigate the dynamic behaviour accurately. Additionally, these components often incorporate cutout openings such as windows, holes, and access cutouts to meet functional and weight requirements, adding complexity to their behaviour and modelling.

Numerous studies have been conducted on the dynamic behaviour of laminated shells the finite element method (FEM), which is widely used in industrial practice, e.g. [2, 3, 4, 5]. However, alternative techniques such as analytical solutions for simple cases [6], the domain decomposition method [7, 8], the wavelet based methods [9, 10, 11], the wave based method [12, 13], the discrete singular convolution method [14, 15], the method of reverberation ray matrix [16], the spectral-Tchebyshev technique [17], and meshless methods [18, 19, 20, 21] can offer valuable insights by providing benchmark solutions and efficient alternatives to finite elements, particularly during the preliminary design phase and optimisation procedures. One such approach is the Ritz method [22], renowned for its computational efficiency in modelling composite structures. It has been successfully employed to analyse the behaviour of cylindrical shells, generally without cutouts, e.g. [23, 24, 25, 26, 27]

In the framework of Ritz approaches, the present work proposes a novel single-domain formulation for free vibration analysis of cylindrical composite shells with cutouts. The plate structural model is based on the first-order shear deformation theory, whose primary variable, namely the shell midplane translation and the shell section rotations, are approximated by a set of trial functions built with orthogonal Legendre polynomials. The stationarity condition of the total energy potential provides the

resolving algebraic system in terms of the primary variables unknown Ritz coefficients. The characteristic matrices of the resolving system are computed using a unique integration technique, which relies on the implicit description of the cutout via a suitably defined level set function. This technique enables an accurate evaluation of domain integrals over the shell domain and constitutes the proposed Ritz approach's core and principal novelty. Validation results and studies demonstrating the potential of this method are presented.

#### 2. Formulation

Let us consider a cylindrical shell panel with rectangular planform, having radius R, panel open angle  $2\alpha$  and length 2L as depicted in Fig. 1. The panel mid-surface occupies the domain  $\Omega$  with boundary  $\partial\Omega$ . It is built as a laminate with general layup having  $N_L$  constant thickness layers of composite material. The panel is generally constrained along its edges.

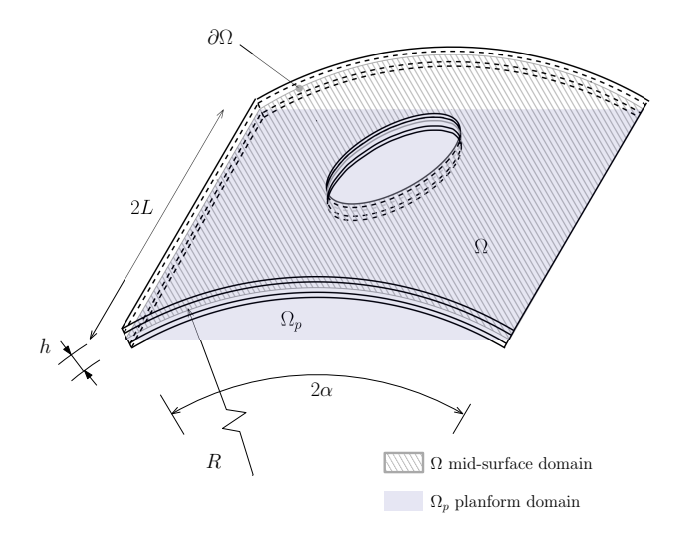


Figure 1 - Cylindrical shell panel geometry.

The panel mid-surface is referred to a Cartesian coordinate system with the  $x_1$  and  $x_2$  axes spanning the rectangular planform domain  $\Omega_p$  and the origin located at the planform domain center. A curvilinear orthogonal coordinate system  $\xi_1, \xi_2, \zeta$  is introduced on the mid-surface being  $\xi_1$  directed along the circumferential direction,  $\xi_2$  parallel to the cylinder axis and  $\zeta$  directed along the normal to the panel mid-surface. Finally, a linear map is established between the curvilinear coordinates  $\xi_1\xi_2$  and the natural coordinates  $\xi$  and  $\eta$ , which span the domain  $Q \equiv [-1,1] \times [-1,1]$ . The Fig. 2 shows the reference systems employed. Accordingly, the panel mid-plane point coordinates are given by

$$\begin{cases} x_1 \\ x_2 \\ x_3 \end{cases} = \begin{cases} R \sin \alpha \xi \\ L \eta \\ R (\cos \alpha \xi - \cos \alpha) \end{cases}$$
 (1)

The panel can present a cutout, obtained by intersecting it with a general section cylinder, having axis directed along the  $x_3$  direction, see Fig. 2. The cut-out geometry is implicitly described via a *level set* function  $\varphi$  provided in terms of the cartesian coordinates  $x_1$  and  $x_2$ , i.e.  $\varphi = \varphi(\mathbf{P}) = \varphi(x_1, x_2)$ . Accordingly, the panel cutted mid-surface domain  $\Omega_c$  is defined as the part of  $\Omega$  where the function  $\varphi$  has negative value, namely

$$\Omega_c \equiv \{(x_1, x_2, x_3) \in \Omega : \varphi(x_1, x_2) < 0\}.$$
(2)

The *level set* function  $\varphi$  also allow to define the cutout boundary  $\Gamma$  as the part of the domain  $\Omega$  where  $\varphi$  is zero

$$\Gamma \equiv \{(x_1, x_2, x_3) \in \Omega : \varphi(x_1, x_2) = 0\}. \tag{3}$$

It is worth noting that the *level set* function  $\varphi$  can be expressed in terms of the curvilinear coordinates  $\xi_1 \xi_2 \zeta$  or natural coordinates  $\xi \eta$  by using the Eq. (1). The Fig. 3 provides some examples of *level set* functions describing typical cutouts.

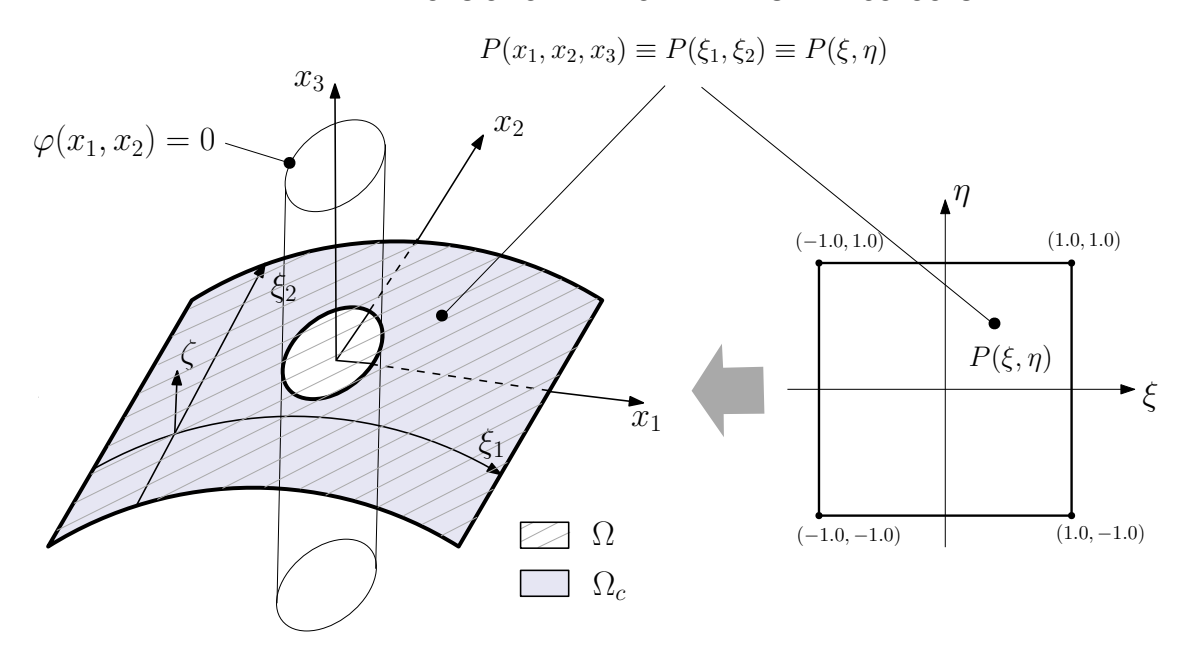


Figure 2 – Cylindrical panel references systems and mapping.

## 2.1 Shell panel kinematics

To describe the panel kinematics, the Fist Order Shear Deformation theory (FSDT) is assumed and the displacement field  $\boldsymbol{d}^T = \left\{ d_{\xi_1} \quad d_{\xi_2} \quad d_{\zeta} \right\}^T$  is given by

$$d = u + \zeta L\vartheta \tag{4}$$

where  $d_{\mu}$ ,  $\mu \in \{\xi_1, \xi_2, \zeta\}$ , are the displacement component along  $\xi_1 \xi_2 \zeta$  axes, and

$$\boldsymbol{L} = \begin{bmatrix} 1 & 0 & 0 \\ 0 & 1 & 0 \end{bmatrix}^T \tag{5}$$

In Eq. (4), the generalized displacement vectors  $\mathbf{u}$  and  $\mathbf{\vartheta}$  are defined as  $\mathbf{u} = \begin{bmatrix} u & v & w \end{bmatrix}^T$  and  $\mathbf{\vartheta} = \begin{bmatrix} \vartheta_{\xi_1} & \vartheta_{\xi_2} \end{bmatrix}^T$  being u and v the in-plane translations of the mid-surface points along the  $\xi_1$  and  $\xi_2$  axes, w the transverse deflection along the  $\zeta$  direction,  $\vartheta_{\xi_1}$  and  $\vartheta_{\xi_2}$  the section rotations around the  $\xi_2$  and  $\xi_1$ -axis, respectively.

The linear strain-displacement relations are written as [28]

$$\boldsymbol{e}_{p} = \begin{cases} e_{11} \\ e_{22} \\ e_{12} \end{cases} = \boldsymbol{\mathscr{Z}}\boldsymbol{\varepsilon} + \zeta \boldsymbol{\mathscr{Z}}\boldsymbol{\kappa} \tag{6a}$$

$$\boldsymbol{e}_n = \begin{Bmatrix} e_{13} \\ e_{23} \end{Bmatrix} = \boldsymbol{\mathscr{Z}}_s \boldsymbol{\gamma} \tag{6b}$$

where the generalized strain vectors  $\boldsymbol{\varepsilon}, \boldsymbol{\kappa}$  and  $\boldsymbol{\gamma}$  are defined as

$$\boldsymbol{\varepsilon} = \begin{bmatrix} \frac{\partial}{\partial \xi_1} & 0 & \frac{1}{R} \\ 0 & \frac{\partial}{\partial \xi_2} & 0 \\ 0 & \frac{\partial}{\partial \xi_1} & 0 \\ \frac{\partial}{\partial \xi_2} & 0 & 0 \end{bmatrix} \begin{Bmatrix} u \\ v \\ w \end{Bmatrix} = \mathcal{D}_{pu} \boldsymbol{u}$$
 (7a)

$$\mathbf{\kappa} = \begin{bmatrix} \frac{\partial}{\partial \xi_1} & 0\\ 0 & \frac{\partial}{\partial \xi_2}\\ 0 & \frac{\partial}{\partial \xi_1}\\ \frac{\partial}{\partial \xi_2} & 0 \end{bmatrix} \begin{Bmatrix} \vartheta_{\xi_1}\\ \vartheta_{\xi_2} \end{Bmatrix} = \mathscr{D}_{pu}\boldsymbol{\vartheta}$$
 (7b)

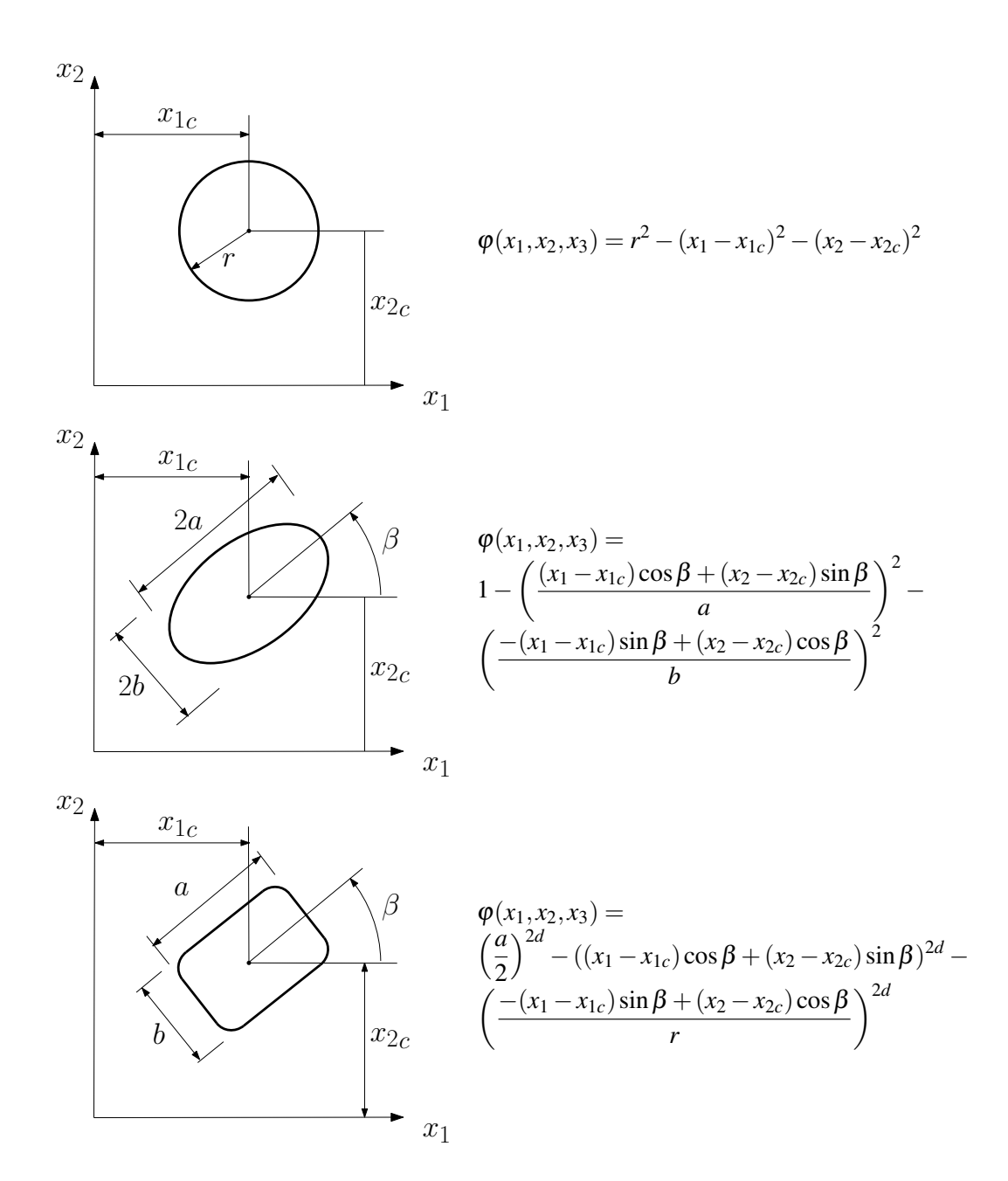


Figure 3 – Level set functions describing typical cutouts.

$$\boldsymbol{\gamma} = \begin{pmatrix} \vartheta_{\xi_1} \\ \vartheta_{\xi_2} \end{pmatrix} + \begin{bmatrix} -\frac{1}{R} & 0 & \frac{\partial}{\partial \xi_1} \\ 0 & 0 & \frac{\partial}{\partial \xi_2} \end{bmatrix} \begin{pmatrix} u \\ v \\ w \end{pmatrix} = \boldsymbol{\vartheta} + \boldsymbol{\mathscr{D}}_{nu} \boldsymbol{u}$$
 (7c)

and

$$\mathbf{Z} = \begin{bmatrix} \frac{1}{(1+\zeta/R)} & 0 & 0 & 0\\ 0 & 1 & 0 & 0\\ 0 & 0 & \frac{1}{(1+\zeta/R)} & 1 \end{bmatrix}$$
(8a)

$$\mathbf{\mathscr{Z}}_{s} = \begin{bmatrix} \frac{1}{(1+\zeta/R)} & 0\\ 0 & 1 \end{bmatrix}$$
 (8b)

# 2.2 Ply constitutive equations

Assuming plane stress ( $\sigma_{33} = 0$ ), the k-th ply constitutive equations are written as

$$\left\{ \begin{array}{l}
 \sigma_{p}^{(k)} \\
 \sigma_{n}^{(k)}
 \end{array} \right\} = \left\{ \begin{array}{l}
 \sigma_{12}^{(k)} \\
 \sigma_{12}^{(k)} \\
 \sigma_{31}^{(k)} \\
 \sigma_{32}^{(k)}
 \end{array} \right\} = \left[ \begin{array}{l}
 \mathbf{Q}_{p}^{(k)} & \mathbf{0} \\
 \mathbf{0} & \mathbf{Q}_{n}^{(k)}
 \end{array} \right] \left\{ \begin{array}{l}
 \mathbf{e}_{p} \\
 \mathbf{e}_{n}
 \end{array} \right\} \tag{9}$$

where the superscript (k) is employed to denote quantities related to the k-th ply. The elements of the ply stiffness matrices  $\mathbf{Q}_p^{(k)}$  and  $\mathbf{Q}_n^{(k)}$  have the following expressions

$$Q_{p_{11}}^{(k)} = \bar{Q}_{11}^{(k)} \cos^4 \theta + 2\left(\bar{Q}_{12}^{(k)} + 2\bar{Q}_{33}^{(k)}\right) \sin^2 \theta \cos^2 \theta + \bar{Q}_{22}^{(k)} \sin^4 \theta \tag{10a}$$

$$Q_{p_{12}(k)} = \bar{Q}_{12}^{(k)} \cos^4 \theta + \left(\bar{Q}_{11}^{(k)} + Q_{22}^{(k)} - 4\bar{Q}_{33}^{(k)}\right) \sin^2 \theta \cos^2 \theta + \bar{Q}_{12}^{(k)} \sin^4 \theta \tag{10b}$$

$$Q_{P22}^{(k)} = \bar{Q}_{11}^{(k)} \sin^4 \theta + 2\left(\bar{Q}_{12}^{(k)} + 2\bar{Q}_{33}^{(k)}\right) \sin^2 \theta \cos^2 \theta + \bar{Q}_{22}^{(k)} \cos^4 \theta \tag{10c}$$

$$Q_{P13}^{(k)} = \left(\bar{Q}_{11}^{(k)} - Q_{12}^{(k)} - 2\bar{Q}_{33}^{(k)}\right)\sin\theta\cos^3\theta + \left(\bar{Q}_{12}^{(k)} - Q_{22}^{(k)} + 2\bar{Q}_{33}^{(k)}\right)\sin^3\theta\cos\theta \tag{10d}$$

$$Q_{p23}^{(k)} = \left(\bar{Q}_{11}^{(k)} - Q_{12}^{(k)} - 2\bar{Q}_{33}^{(k)}\right)\sin^3\theta\cos\theta + \left(\bar{Q}_{12}^{(k)} - Q_{22}^{(k)} + 2\bar{Q}_{33}^{(k)}\right)\sin\theta\cos^3\theta \tag{10e}$$

$$Q_{P33}^{(k)} = \left(\bar{Q}_{11}^{(k)} + Q_{22}^{(k)} - 2\bar{Q}_{12}^{(k)} - 2\bar{Q}_{66}^{(k)}\right)\sin^2\theta\cos^2\theta + \bar{Q}_{33}^{(k)}\left(\sin^4\theta + \cos^4\theta\right)\cos\theta \tag{10f}$$

$$Q_{n_{11}}^{(k)} = \bar{Q}_{44}^{(k)} \cos^2 \theta + \bar{Q}_{55}^{(k)} \sin^2 \theta \tag{10g}$$

$$Q_{n12} = \left(\bar{Q}_{55}^{(k)} - \bar{Q}_{44}^{(k)}\right) \cos\theta \sin\theta \tag{10h}$$

$$Q_{n22}^{(k)} = \bar{Q}_{44}^{(k)} \sin^2 \theta + \bar{Q}_{55}^{(k)} \cos^2 \theta \tag{10i}$$

where  $\theta$  is the stacking angle, measured with respect to the  $\xi_1$ -axis, and

$$\bar{Q}_{11} = \frac{E_1}{1 - v_{12}v_{21}} \tag{11a}$$

$$\bar{Q}_{22} = \frac{E_2}{1 - v_{12}v_{21}} \tag{11b}$$

$$\bar{Q}_{12} = \frac{v_{12}E_2}{1 - v_{12}v_{21}} \tag{11c}$$

$$\bar{Q}_{66} = G_{12} \tag{11d}$$

$$\bar{Q}_{44} = G_{23}$$
 (11e)

$$\bar{Q}_{44} = G_{13}$$
 (11f)

being  $E_i$  the Young's moduli,  $G_{ij}$  the shear moduli and  $v_{ij}$  the Poisson' coefficients in the material orthotropic reference system.

# 2.3 Equilibrium and governing equation

Assuming the kinematical boundary conditions are satisfied the equilibrium governing equations for the free vibrations problem can be deduced from the stationarity conditions of the following energy potential [31]

$$\Pi = \int_{\Omega_{c}} \sum_{k=1}^{N_{L}} \int_{h_{k-1}}^{h_{k}} \frac{1}{2} \left[ \boldsymbol{e}_{p}^{T} \boldsymbol{Q}_{p}^{\langle k \rangle} \boldsymbol{e}_{p} + \boldsymbol{e}_{n}^{T} \boldsymbol{Q}_{n}^{\langle k \rangle} \boldsymbol{e}_{n}^{\langle k \rangle} \right] \left( 1 + k_{1} \bar{\zeta} \right) \left( 1 + k_{2} \bar{\zeta} \right) d\zeta d\Omega - \\
\omega^{2} \int_{\Omega_{c}} \sum_{k=1}^{N_{L}} \int_{h_{k-1}}^{h_{k}} \frac{1}{2} \left[ \boldsymbol{\rho}^{(k)} \boldsymbol{d}^{T} \boldsymbol{d} \right] \left( 1 + k_{1} \bar{\zeta} \right) \left( 1 + k_{2} \bar{\zeta} \right) d\zeta d\Omega = \\
= \int_{\Omega_{c}} \frac{1}{2} \left[ \boldsymbol{\varepsilon}^{T} \boldsymbol{A} \, \boldsymbol{\varepsilon} + \boldsymbol{\varepsilon}^{T} \boldsymbol{B} \, \boldsymbol{\kappa} + \boldsymbol{\kappa}^{T} \boldsymbol{B} \, \boldsymbol{\varepsilon} + \boldsymbol{\kappa}^{T} \boldsymbol{D} \, \boldsymbol{\kappa} + \boldsymbol{\gamma}^{T} \boldsymbol{A}_{S} \, \boldsymbol{\gamma} \right] d\Omega - \\
\omega^{2} \int_{\Omega_{c}} \frac{1}{2} \left[ \boldsymbol{u}^{T} \boldsymbol{I}_{uu} \boldsymbol{u} + \boldsymbol{u}^{T} \boldsymbol{I}_{u\vartheta} \, \boldsymbol{\vartheta} + \boldsymbol{\vartheta}^{T} \boldsymbol{I}_{\vartheta u} \boldsymbol{u} + \boldsymbol{\vartheta}^{T} \boldsymbol{I}_{\vartheta \vartheta} \, \boldsymbol{\vartheta} \right] d\Omega$$
(12)

where  $\omega$  is the natural circular frequency,  $h_{k-1}$  and  $h_k$  are the  $\zeta$  coordinates of the k-th ply bottom and top faces, and  $\rho^{(k)}$  is the ply density. The panel stiffness and inertia matrices involved in Eq. (12) are given by

$$\langle \boldsymbol{A}, \boldsymbol{B}, \boldsymbol{D} \rangle = \sum_{k=1}^{N_L} \int_{h_{k-1}}^{h_k} \boldsymbol{\mathscr{Z}}^T \boldsymbol{Q}_p^{\langle k \rangle} \langle 1, \zeta, \zeta^2 \rangle \, \boldsymbol{\mathscr{Z}} (1 + \zeta/R) \, d\zeta \tag{13a}$$

$$\boldsymbol{A}_{S} = \sum_{k=1}^{N_{L}} \int_{h_{k-1}}^{h_{k}} \boldsymbol{\mathcal{Z}}_{S}^{T} \boldsymbol{Q}_{S}^{\langle k \rangle} \boldsymbol{\mathcal{Z}}_{S} \ (1 + \zeta/R) \, d\zeta \tag{13b}$$

$$\langle \mathbf{I}_{uu}, \mathbf{I}_{u\vartheta}, \mathbf{I}_{\vartheta u}, \mathbf{I}_{\vartheta u}, \mathbf{I}_{\vartheta \vartheta} \rangle = \sum_{k=1}^{N_L} \int_{h_{k-1}}^{h_k} \rho^{(k)} \langle \mathbf{I}_{3\times 3}, \zeta \mathbf{L}, \zeta \mathbf{L}^T, \zeta^2 \mathbf{L}^T \mathbf{L} \rangle (1 + \zeta/R) d\zeta$$
(13c)

being  $I_{3\times3}$  the  $3\times3$  identity matrix.

## 3. Ritz solution

The cylindrical panel model introduced in the preceding section is solved by a Ritz approach [22, 29, 30, 32, 31]

## 3.1 Generalized displacements and strains approximation

The shell generalized displacements u and  $\vartheta$ , namely the problem primary variables, are approximated by series of trial function and they are conveniently written in matrix form as

$$\mathbf{u} = \begin{bmatrix} \mathbf{\Psi}_{u} & \mathbf{0} & \mathbf{0} \\ \mathbf{0} & \mathbf{\Psi}_{v} & \mathbf{0} \\ \mathbf{0} & \mathbf{0} & \mathbf{\Psi}_{w} \end{bmatrix} \begin{Bmatrix} \mathbf{C}_{u} \\ \mathbf{C}_{v} \\ \mathbf{C}_{w} \end{Bmatrix} = \mathbf{\Phi}_{u} \mathbf{U}$$
 (14a)

$$\boldsymbol{\vartheta} = \begin{bmatrix} \boldsymbol{\Psi}_{\vartheta_x} & \boldsymbol{0} \\ \boldsymbol{0} & \boldsymbol{\Psi}_{\vartheta_y} \end{bmatrix} \begin{Bmatrix} \boldsymbol{C}_{\vartheta_x} \\ \boldsymbol{C}_{\vartheta_y} \end{Bmatrix} = \boldsymbol{\Phi}_{\vartheta} \boldsymbol{\Theta}$$
 (14b)

where the row vectors  $\Psi_{\tau}$ , with  $\tau \in \{u, v, w, \vartheta_x, \vartheta_y\}$ , and the column vectors  $C_{\tau}$  contain the employed trial functions  $\chi_i$  and the corresponding unknown coefficients, respectively. In the present work, the trial functions used for the approximation of the primary variable are built basing on the tensor product of one-dimensional polynomials [32]. In particular, the generic trial function  $\chi_i$  is defined as

$$\chi_i = f_{\gamma}(\xi, \eta)\phi_m(\xi)\psi_n(\eta) \tag{15}$$

where  $\phi_m(\xi)$  and  $\chi_n(\eta)$  are one-dimensional Legendre orthogonal polynomials of order m and n, respectively. The so-called boundary function  $f_{\chi}$  is chosen to ensure the fulfillment of the homogeneous essential boundary conditions and is defined as

$$f_{\chi}(\xi,\eta) = (1+\xi)^{a_1}(1-\xi)^{a_2}(1+\eta)^{a_3}(1-\eta)^{a_4}$$
(16)

where the exponents  $a_i$  take the value 0 or 1 according to the condition of constrained or unknown value of  $\chi$  along the edge implicitly described by the corresponding power base, see Table 1.

Table 1 – Possible combination of the exponents in Eq.(16).

| Edge                      | Free      | Constrained |  |  |
|---------------------------|-----------|-------------|--|--|
| $(1+\xi)=0$               | $a_1 = 0$ | $a_1 = 1$   |  |  |
| $(1-\xi)=0$               | $a_2 = 0$ | $a_2 = 1$   |  |  |
| $(1+\boldsymbol{\eta})=0$ | $a_3 = 0$ | $a_3 = 1$   |  |  |
| $(1-\eta)=0$              | $a_4 = 0$ | $a_4 = 1$   |  |  |

Accordingly, the discretized form of the generalized strain reads as

$$\boldsymbol{\varepsilon} = \boldsymbol{\mathscr{D}}_{pu} \boldsymbol{\Phi}_{u} \boldsymbol{U} = \boldsymbol{\mathscr{B}}_{pu} \boldsymbol{U} \tag{17a}$$

$$\mathbf{K} = \mathcal{D}_{pu}\mathbf{\Phi}_{\vartheta}\mathbf{\Theta} = \mathcal{B}_{p\vartheta,\vartheta}\mathbf{\Theta} \tag{17b}$$

$$\boldsymbol{\gamma}_0 = \boldsymbol{\Phi}_{\boldsymbol{\vartheta}} \boldsymbol{\Theta} + \boldsymbol{\mathcal{D}}_{nu} \boldsymbol{\Phi}_u \boldsymbol{U} = \boldsymbol{\Phi}_{\boldsymbol{\vartheta}} \boldsymbol{\Theta} + \boldsymbol{\mathcal{B}}_{nu} \boldsymbol{U} \tag{17c}$$

# 3.2 Governing equations

The discrete system governing equations are obtained from the stationarity condition with respect to the Ritz coefficients of the discrete version of the functional  $\Pi$ . This is obtained introducing the Ritz approximation, namely Eqs. (14) and (17) into Eq. (12) and applying the classical variational calculus procedures. Finally, the following resolving system is obtained

$$(\mathbf{K} - \omega^2 \mathbf{M}) \mathbf{X} \tag{18}$$

where  $\mathbf{X}^T = \left\{ \mathbf{U}^T \quad \mathbf{\Theta}^T \right\}^T$  is the vector containing the Ritz unknown coefficients,  $\mathbf{K}$  is the stiffness matrix and  $\mathbf{M}$  is the mass matrix. The mass and stiffness matrices involved in Eq. (18) are defined by

$$\mathbf{M} = \begin{bmatrix} \int_{\Omega_c} \mathbf{\Phi}_u^T \mathbf{I}_{uu} \mathbf{\Phi}_u d\Omega & \int_{\Omega_c} \mathbf{\Phi}_u^T \mathbf{I}_{u\vartheta} \mathbf{\Phi}_{\vartheta} d\Omega \\ \int_{\Omega_c} \mathbf{\Phi}_{\vartheta}^T \mathbf{I}_{\vartheta u} \mathbf{\Phi}_u d\Omega & \int_{\Omega_c} \mathbf{\Phi}_{\vartheta}^T \mathbf{I}_{\vartheta \vartheta} \mathbf{\Phi}_{\vartheta} d\Omega \end{bmatrix}$$
(19)

$$\mathbf{K} = \begin{bmatrix} \mathbf{K}_{uu} & \mathbf{K}_{u\vartheta} \\ \mathbf{K}_{\vartheta u} & \mathbf{K}_{\vartheta\vartheta} \end{bmatrix}$$
 (20)

where

$$\mathbf{K}_{uu} = \int_{\Omega_{-}} \left[ \mathbf{B}_{pu}^{T} \mathbf{A} \mathbf{B}_{pu} + \mathbf{B}_{nu}^{T} \mathbf{A}_{S} \mathbf{B}_{nu} \right] d\Omega$$
 (21a)

$$\mathbf{K}_{u\vartheta} = \mathbf{K}_{\vartheta u}^{T} = \int_{\Omega_{c}} \left[ \mathcal{B}_{pu}^{T} \mathbf{B} \mathcal{B}_{p\vartheta} + \mathcal{B}_{nu}^{T} \mathbf{A}_{S} \mathbf{L} \mathbf{\Phi}_{\vartheta} \right] d\Omega$$
 (21b)

$$\mathbf{K}_{\vartheta\vartheta} = \int_{\Omega_{\sigma}} \left[ \mathbf{B}_{p\vartheta}^{T} \mathbf{D} \mathbf{B}_{p\vartheta} + \mathbf{\Phi}_{\vartheta}^{T} \mathbf{L}^{T} \mathbf{A}_{S} \mathbf{L} \mathbf{\Phi}_{\vartheta} \right] d\Omega \tag{21c}$$

The Eq. (18) identifies a linear algebraic eigenvalue problem whose solution provides the panel natural circular frequencies and the corresponding Ritz coefficients that via Eq.(14) enable the mode shape reconstruction.

# 4. Stiffness and mass matrix computation

The calculation of the mass and stiffness matrices requires the evaluation of complex domain integrals, as shown in the Eqs. (19) and (20). In the most general case, such integrals cannot be evaluated analytically and require the introduction of appropriate numerical integration or quadrature techniques. In this work, exploiting the implicit description of the cutout via a level set function, high-order quadrature rules obtained using the algorithm developed in [33] are employed coupled with an adaptive subregioning scheme to improve the integration effectiveness.

As discussed in Sec. 2.it was assumed that a generic point on the panel mid-surface can be represented using a system of natural coordinates  $(\xi,\eta)$  defined in the square domain  $Q\equiv [-1,1]\times [-1,1]$  through Eq. (1). Assuming then that the domain  $\Omega_S$  is a generic subregion of the panel mid-surface, such *mapping* allows the integral of the generic function f on  $\Omega_S$  to be expressed as

$$\int_{\Omega_{S}} f(\mathbf{P}) d\Omega = \int_{\widetilde{\Omega}_{S}} f[\mathbf{P}(\xi, \eta)] J(\xi, \eta) d\Omega$$
 (22)

here  $J(\xi,\eta)$  is the determinant of the Jacobian matrix of the mapping employed and  $\widetilde{\Omega}_s$  is a subregion of the square domain Q such that the points  $(\xi,\eta)\in\widetilde{\Omega}_s$  are mapped into  $\Omega_s$ . The numerical evaluation of the second-member integral of Eq.(22) is written as

$$\int_{\widetilde{\Omega}_S} f[\mathbf{P}(\xi, \eta)] J(\xi, \eta) d\Omega = \sum_{g=1}^{N_g} f^g J^g w^g$$
(23)

where  $f^g$  represents the value of the function f evaluated at the integration point defined by the natural coordinates  $(\xi^g, \eta^g)$ ,  $J^g$  represents the value of  $J(\xi, \eta)$  evaluated at the integration point,  $w^g$  represents the weight of the integration point, and  $N_g$  is the total number of integration points. The set of integration points and their weights is the *quadrature rule* for the domain  $\widetilde{\Omega}_c$ .

## 4.1 Panel without cutout

For panels without cutout, the computation of the mass and stiffness matrices is obtained by evaluating integrals of the form introduced in the Eqs. (22) and (23) where the  $\Omega_S$  domain coincides with the  $\Omega$  domain of the panel and, consequently, the  $\widetilde{\Omega}_S$  domain coincides with the Q square domain. In this case, the integration points and weights are provided by the tensor product of one-dimensional Gauss guadrature rules.

## 4.2 Panel with cutout

In the case of panels with cutout, the domain  $\Omega_S$  coincides with  $\Omega_c$  and then the domain  $\Omega_S$  coincides with a subset of Q, as shown in Fig.4. In the present formulation, the domain  $\Omega_c$  is defined by a

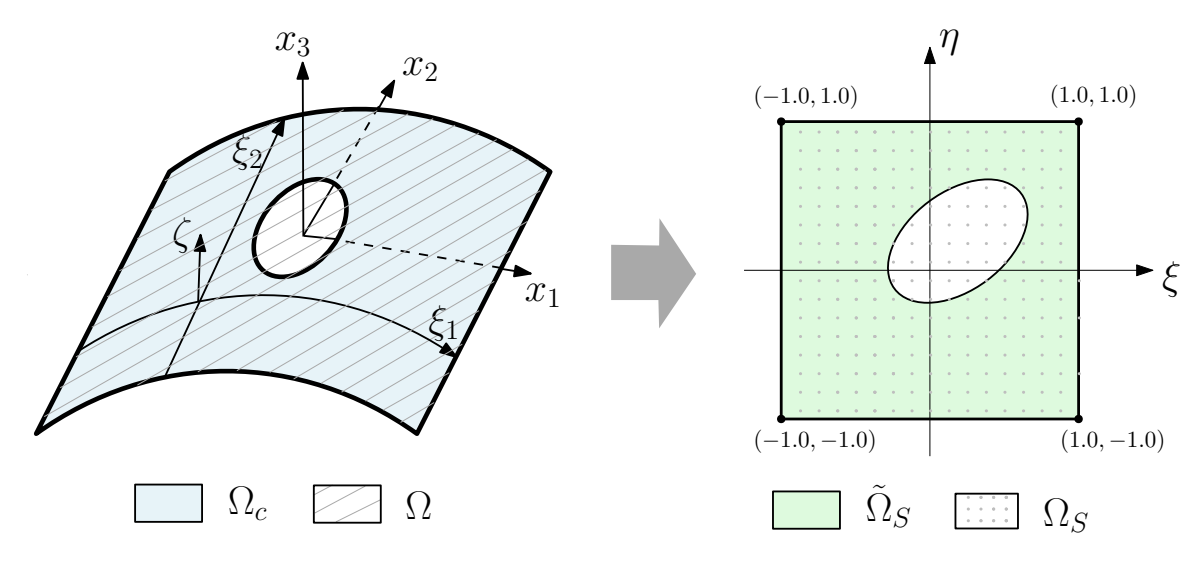


Figure 4 – Mapping of a cylindrical panel with cutout.

function *level set*  $\varphi$ , see Eq. (2), which can be expressed as a function of the natural coordinates  $(\xi, \eta)$  by introducing a companion *level set* function  $\widetilde{\varphi}$  as follows

$$\widetilde{\varphi}(\xi,\eta) \equiv \varphi(\mathbf{P}(\xi,\eta)).$$
 (24)

Once the function *level set*  $\widetilde{\varphi}$  is defined in the square domain Q, it is possible to apply the algorithm for computing quadrature rules for implicitly defined domains developed in Ref.[33, 34, 35], whose steps are recalled in the following. The first step is to partition the Q domain of the natural variables  $(\xi, \eta)$  into a set of subdomains that verify one of the following conditions:

- a) the *level set* function  $\widetilde{\varphi}$  is always negative;
- b) the *level set* function  $\widetilde{\varphi}$  is always positive;
- c) the *level set* function  $\widetilde{\varphi}$  changes sign but its gradient in the  $\xi$  direction, defined as  $g_{\equiv}\partial\widetilde{\varphi}/\partial xi$ , or the gradient in the  $\eta$  direction, defined as  $g_{\equiv}\partial\widetilde{\varphi}/\partial\eta$ , is always positive or negative.

This partitioning starts from the square domain Q and is done recursively, checking the sign of  $\widetilde{\varphi}$ ,  $g_{\xi}$  and  $g_{\eta}$ . If none of the conditions a), b) or c) is met, the domain Q is subdivided into two subdomains  $Q_1$  and  $Q_2$ ; the direction of subdivision is chosen along the direction for which the gradient of  $\widetilde{\varphi}$  is smaller. The conditions a), b) or c) for the domains  $Q_1$  and  $Q_2$  are then checked, repeating the steps just described for the domain Q.

As the generic subdomain  $Q_k$  verifies one of the conditions a), b) or c), the following cases can occur

- in the case of a, the subdomain  $Q_k$  falls outside the *cutout* and entirely within the panel domain; the integration points and weights are computed using the tensor product of the one-dimensional Gauss quadrature rules.
- in the case of b, the subdomain  $Q_k$  falls within the *cutout* and entirely outside the panel domain, not contributing to the domain integrals; its integration points and weights thus constitute an empty set.
- in the case of c, the subdomain  $Q_k$  intersects the boundary of the *level set* function. However, the condition that, for example, the gradient  $g_{\xi}$  always has the same sign ensures that, for given  $\eta$ , the function  $\widetilde{\varphi}$  is always increasing or decreasing and thus has at most one zero. On the basis of these observations, and assuming that the subdomain  $Q_k$  is identified by  $Q_k \equiv [\xi^L, \xi^U] \times [\eta^L, \eta^U]$ , the computation of the quadrature rule consists of the following steps:
  - 1. Compute all the zeros of the function  $\widetilde{\varphi}(\xi = \xi^L, \eta)$  and of the function  $\widetilde{\varphi}(\xi = \xi^U, \eta)$ .
  - 2. Create an ordered list of  $\eta$  coordinates where the first value coincides with  $\eta^L$ , the last value coincides with  $\eta^U$ , and the interior values coincide with the zeros just computed; assuming that n zeros have been computed, the list can be identified by the ordered set  $\{\eta_0, \ldots, \eta_{n+1}\}$  where  $\eta_0 = \eta^L$  and  $\eta_{n+1} = \eta^U$
  - 3. Define a set of intervals  $I^i_{\eta} \equiv [\eta_{i-1}, \eta_i]$ , with  $i = 1, \dots, n+1$ .
  - 4. The integral of a generic function f on  $Q_k$  can then be written as follows.

$$\int_{Q_k} f(\xi, \eta) \, d\xi \, d\eta = \sum_{i=1}^{n+1} \int_{I_{\eta}^i} \hat{f}(\eta) \, d\eta \tag{25}$$

where

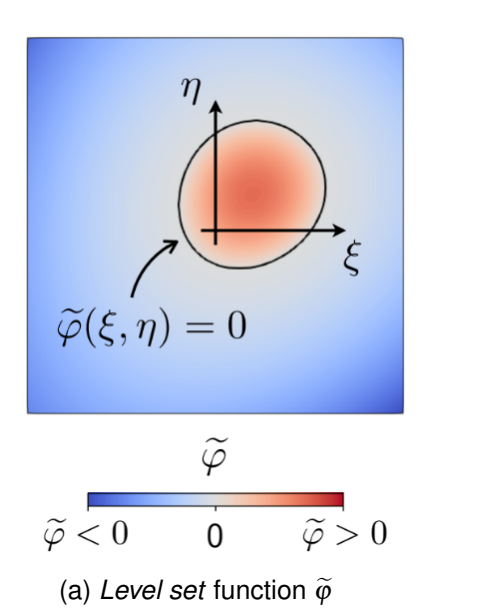
$$\hat{f}(\eta) \equiv \int_{I_{\xi}(\eta)} f(\xi, \eta) \,\mathrm{d}\xi. \tag{26}$$

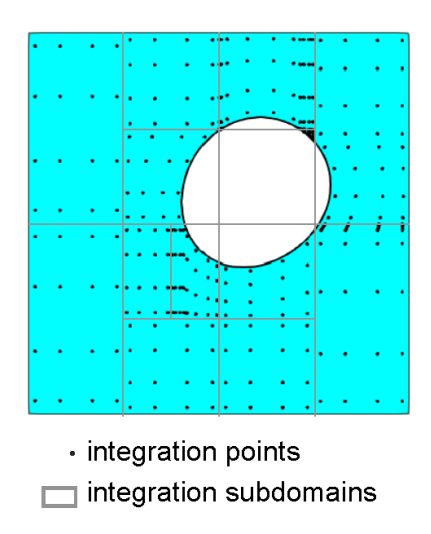
The interval  $I_{\xi}(\eta)$  in the above equation represents the segment of  $Q_k$  at  $\eta$  fixed where  $\widetilde{\varphi}$  is negative. Recalling that  $g_{\xi}$  is always of the same sign, if  $\widetilde{\varphi}(\xi,\eta)$  has a zero  $\xi_k$  and  $g_{\xi}>0$ , the interval coincides with  $I_{\xi}(\eta)\equiv [\xi^L,\xi_k]$ ; if  $\widetilde{\varphi}(\xi,\eta)$  has a zero  $\xi_k$  and  $g_{\xi}<0$ , the interval coincides with  $I_{\xi}(\eta)\equiv [\xi_k,\xi^U]$ ; on the other hand, if  $\widetilde{\varphi}(\xi,\eta)$  has no zeros, the interval coincides with  $I_{\xi}(\eta)\equiv [\xi^L,\xi^U]$ . Thus, using one-dimensional Gauss quadrature for each interval  $I_{\eta}^i$  and one-dimensional Gauss quadrature for each interval  $I_{\xi}(\eta)$  associated with the integration point  $\eta\in I_{\eta}^i$ , it is possible to compute the integration points and corresponding weights for the domain  $Q_k$ .

As an example, the Fig. 5b shows the integration subdomains and quadrature points computed via the above-described procedure foe the domain described by the *level set* function shown in Fig. 5a

## 5. Numerical results

A computer code has been implemented to validate the formulation described in the previous sections. To this aim tests involving a multilayered cylindrical shell panel having radius  $R=0.25\,\mathrm{m}$  and a square planform with edge length  $L=0.4\,\mathrm{m}$  are carried out. The ply thickness and material properties are are listed in Table 2. Different cutouts, layups and boundary conditions are considered to assess the capabilities of the proposed approach in ascertaining the free vibrations of cylindrical panels with cutouts.





(b) Subdomains and quadrature points

Figure 5 – Integration subdomains and quadrature points computed for the domain implicitly described by the *level set* function  $\widetilde{\varphi}$ .

Table 2 – Properties of the materials and stacking sequence

| Property   |   | Value   |
|--|---|---|
| Young's moduli   | $E_1 \\ E_2, E_3$                               | 113.0 [GPa]<br>9.0 [GPa]  |
| Poisson's ratios<br>Shear moduli<br>Mass density<br>Layers thickness | $v_{12} \\ G_{23}, G_{13}, G_{12} \\ \rho \\ t$ | 0.302<br>3.82 [GPa]<br>1540.0 [kg/m <sup>3</sup> ]<br>0.002 [m] |

Preliminarily, representative convergence analysis results are presented and discussed for the case of a fully clamped panel with [0/90/90/0] layup and a central circular cutout having radius  $r=0.075\,\mathrm{m}$ . The analyses have been carried out employing trial functions built as in Eq. (15) with m and n running in the set  $\{1,2,...,N\}$ . The same approximation order N is used for all the primary variables and this approximation scheme is denoted as  $R_{N\times N}$ . Table 3 lists the convergence study results for the first six circular natural frequencies  $\omega$  of the panel. Reference results are also listed and used to calculate the percentage error; they have been obtained using a finite element model with 29600 four node quadrilateral elements. The results evidence good convergence properties of the proposed method and a very good agreement with finite element results.

To illustrate the method capability to accurately ascertain the panel free vibrations, studies have been performed for different configurations. Table 4 lists the circular frequency of the [0/90/90/0] composite cylindrical panel subjected to different edges kinematical constraints. In particular, fully clamped (CCCC), fully simply-supported (SSSS) and cantilever (CFFF) configurations have been analyzed. The comparison of the present results with those of converged finite element analyses shows the accuracy of the present solution with respect to different kinematical boundary conditions.

Table 5 lists the circular frequency of the fully clamped panel with different stacking sequences, namely a four ply cross-ply layup, a four ply non symmetric layup and an eight ply symmetric layup. The results obtained are compared with converged finite element results showing very good agreement and validating the approach with respect the layup parameters. It is worth noting that to achieve the same level of accuracy for all of the investigated layups, the  $R_{32\times32}$  approximation scheme was used and this is related to the unsymmetric layup results whose vibration behaviour accurate descrip-

tion claims for a finer discretization.

Table 3 – [0/90/90/0] laminated cylindrical panel with a central circular cutout: natural circular frequencies  $\omega$  convergence study.

|          | FEM    | $R_{16x16}$ |         | $R_{2}$ | 4 <i>x</i> 24 | $R_3$  | $R_{32x32}$ |  |
|----------|--------|-------------|---------|---------|---------------|--------|-------------|--|
| Mode nr. | ω      | ω           | % error | ω       | % error       | ω      | % error     |  |
| 1        | 6136.6 | 6188.8      | 0.85%   | 6150.8  | 0.23%         | 6141.9 | 0.09%       |  |
| 2        | 6888.9 | 6946.6      | 0.84%   | 6900.4  | 0.17%         | 6893.8 | 0.07%       |  |
| 3        | 8506.9 | 8597.4      | 1.06%   | 8518.3  | 0.13%         | 8508.1 | 0.01%       |  |
| 4        | 8754.6 | 9030.9      | 3.16%   | 8793.9  | 0.45%         | 8762.5 | 0.09%       |  |
| 5        | 9430.0 | 9515.9      | 0.91%   | 9449.4  | 0.21%         | 9437.7 | 0.08%       |  |
| 6        | 9547.9 | 9929.1      | 3.99%   | 9589.4  | 0.43%         | 9557.6 | 0.10%       |  |

Table 4 – [0/90/90/0] laminated cylindrical panel with a central circular cutout and different edge constraints (CCCC, SSSS, CFFF): circular frequencies  $\omega$  of the first six natural modes.

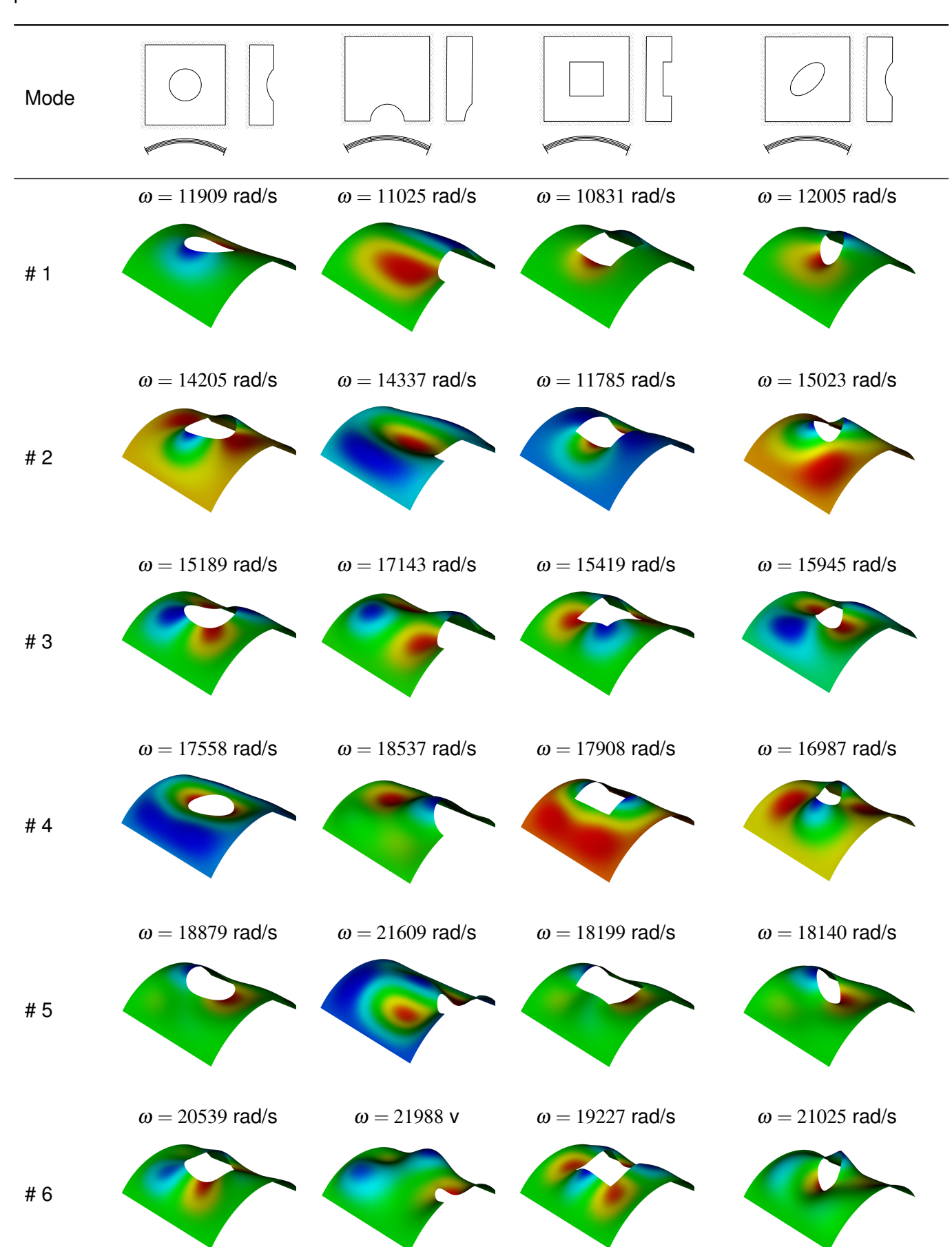
|        |             | CCCC   |         |             | SSSS   |         |             | CFFF   |         |
|--------|-------------|--------|---------|-------------|--------|---------|-------------|--------|---------|
|        | $R_{24x24}$ | FEM    | error % | $R_{24x24}$ | FEM    | error % | $R_{24x24}$ | FEM    | error % |
| Mode 1 | 6150.8      | 6136.6 | 0.23%   | 5342.0      | 5339.2 | 0.05%   | 913.0       | 912.0  | 0.11%   |
| Mode 2 | 6900.4      | 6888.9 | 0.17%   | 5554.7      | 5545.0 | 0.17%   | 1018.7      | 1018.3 | 0.07%   |
| Mode 3 | 8518.3      | 8506.9 | 0.13%   | 6833.1      | 6827.3 | 0.08%   | 2501.5      | 2496.2 | 0.22%   |
| Mode 4 | 8793.9      | 8754.6 | 0.45%   | 7464.4      | 7438.2 | 0.35%   | 2501.6      | 2497.0 | 0.18%   |
| Mode 5 | 9449.4      | 9430.0 | 0.21%   | 7786.2      | 7773.1 | 0.17%   | 3331.1      | 3329.5 | 0.06%   |
| Mode 6 | 9589.4      | 9547.9 | 0.43%   | 8415.2      | 8380.7 | 0.41%   | 3488.6      | 3488.5 | 0.02%   |

Table 5 – Fully clamped (CCCC) laminated cylindrical panel with a central circular cutout and different layups: circular frequencies  $\omega$  of the first six natural

|        | [90/0/0/90] |      |         | [0          | [0/45/-45/90] |         |             | [0/45/-45/90] <sub>S</sub> |         |  |
|--------|-------------|------|---------|-------------|---------------|---------|-------------|----------------------------|---------|--|
|        | $R_{32x32}$ | FEM  | error % | $R_{32x32}$ | FEM           | error % | $R_{32x32}$ | FEM                        | error % |  |
| Mode 1 | 6142        | 6137 | 0.09%   | 8247        | 8245          | 0.02%   | 11909       | 11919                      | -0.08%  |  |
| Mode 2 | 6894        | 6889 | 0.07%   | 8775        | 8700          | 0.87%   | 14205       | 14246                      | -0.29%  |  |
| Mode 3 | 8508        | 8507 | 0.01%   | 9844        | 9821          | 0.23%   | 15189       | 15260                      | -0.47%  |  |
| Mode 4 | 8762        | 8755 | 0.09%   | 10445       | 10361         | 0.81%   | 17558       | 17607                      | -0.28%  |  |
| Mode 5 | 9438        | 9430 | 0.08%   | 10586       | 10510         | 0.72%   | 18879       | 18965                      | -0.45%  |  |
| Mode 6 | 9558        | 9548 | 0.10%   | 11080       | 10936         | 1.32%   | 20539       | 20626                      | -0.42%  |  |

Finally, to illustrate the method's capability in dealing with different cutout shapes and positions, Tab. 6 reports the natural circular frequencies and associated modal shapes for the clamped cylindrical panel with  $[0/45/-45/90]_S$  layup and different cutouts. Analyses refer to a central circular cutout with radius  $r = 0.075 \, m$ ; an edge semicircular cutout with radius  $r = 0.075 \, m$ , a central square cutout with edge length  $a = 0.075 \, m$  and a central,  $45^{\circ}$  inclined, elliptical cutout with axes length  $a = 0.15 \, m$  and  $b = 0.075 \, m$ ; for a geometrical sketch of the investigated cutouts refer to the first row of Tab. 6. The presented results have been obtained by the  $R_{32\times32}$  discretization scheme, which provides converged solution. They show the proposed method's ability in analyzing cylindrical panels with cutouts and can provide a useful benchmark.

Table 6 – Free vibrations circular frequencies and modal shapes for the  $[0/45/-45/90]_S$ , fully clamped panel with different cutouts.



## 6. Conclusions

In this work, a single-domain Ritz method for the free-vibration analysis of laminated composite cylindrical panels with cutouts has been proposed. In the framework of the first order shear deformation theory, the presence of the cut-out is resolved through an implicit approach, whereby a level-set function, that implicitly defines the reference domain, is combined with an efficient quadrature algorithm to compute the resolving system matrices. The formulation has been assessed through multiple tests employed to study its convergence characteristics and accuracy features with respect to edge constraints, layups and cutout shape and position. In general, in all the conducted tests, the results obtained show very good agreement with finite elements reference solutions; demonstrating the potential of the formulation for being used as an effective tool for the free-vibration analysis of cylindrical panels.

## 7. Contact Author Email Address

mailto: alberto.milazzo@unipa.it

# 8. Copyright Statement

The authors confirm that they, and/or their company or organization, hold copyright on all of the original material included in this paper. The authors also confirm that they have obtained permission, from the copyright holder of any third party material included in this paper, to publish it as part of their paper. The authors confirm that they give permission, or have obtained permission from the copyright holder of this paper, for the publication and distribution of this paper as part of the ICAS proceedings or as individual off-prints from the proceedings.

## References

- [1] Carrera E, Zappino E. Carrera Unified Formulation for Free-Vibration Analysis of Aircraft Structures. *AIAA Journal*, Vol. 54, No. 1, pp 280-292, 2016.
- [2] Caliri M F, Ferreira A J M , Tita V, A review on plate and shell theories for laminated and sandwich structures highlighting the Finite Element Method, *Composite Structures*, Vol. 156, pp 63-77, 2016.
- [3] Chakravorty, Dipankar, P. K. Sinha, and J. N. Bandyopadhyay. Applications of FEM on free and forced vibration of laminated shells. *Journal of Engineering Mechanics*, Vol. 124, No. 1, pp 1-8, 1998.
- [4] Hirwani, C. K., Patil, R. K., Panda, S. K., Mahapatra, S. S., Mandal, S. K., Srivastava, L., Buragohain, M. K. Experimental and numerical analysis of free vibration of delaminated curved panel. *Aerospace Science and Technology*, Vol. 54, pp 353-370, 2016.
- [5] Dey, S., Karmakar, A. Free vibration analyses of multiple delaminated angle-ply composite conical shells A finite element approach. *Composite structures*, Vol. 94, No. 7, pp 2188-2196, 2012.
- [6] Shakouri, M., Kouchakzadeh, M. A. Analytical solution for vibration of generally laminated conical and cylindrical shells. *International Journal of Mechanical Sciences*, Vol. 131, pp 414-425, 2017.
- [7] Qu, Y., Hua, H., Meng, G. A domain decomposition approach for vibration analysis of isotropic and composite cylindrical shells with arbitrary boundaries. *Composite structures*, Vol. 95, pp 307-321, 2013.
- [8] Qu, Y., Long, X., Wu, S., Meng, G. A unified formulation for vibration analysis of composite laminated shells of revolution including shear deformation and rotary inertia. *Composite structures*, Vol. 98, pp 169-191 (2013).
- [9] Xiang, X., Guoyong, J., Wanyou, L., Zhigang, L. A numerical solution for vibration analysis of composite laminated conical, cylindrical shell and annular plate structures. *Composite structures*, Vol. 111, pp 20-30, 2014.
- [10] Xie, X., Jin, G., Yan, Y., Shi, S. X., Liu, Z. Free vibration analysis of composite laminated cylindrical shells using the Haar wavelet method. *Composite structures*, Vol. 109, pp 169-177, 2014.
- [11] Zuo, H., Chen, Y., Jia, F., Yang, Z. Unified wavelet finite element formulation for static and vibration analysis of laminated composite shells. *Composite structures*, Vol. 272, 114207, 2021.
- [12] He, D., Shi, D., Wang, Q., Shuai, C. Wave based method (WBM) for free vibration analysis of cross-ply composite laminated cylindrical shells with arbitrary boundaries. *Composite structures*, Vol. 213, pp 284-298, 2019.
- [13] Liu, T., Wang, A., Wang, Q., Qin, B. Wave based method for free vibration characteristics of functionally graded cylindrical shells with arbitrary boundary conditions. *Thin-Walled Structures*, Vol. 148, 106580, 2020.

- [14] Civalek, Ö. Numerical analysis of free vibrations of laminated composite conical and cylindrical shells: discrete singular convolution (DSC) approach. *Journal of Computational and Applied Mathematics*, Vol. 205, No. 1, pp 251-271, 2007.
- [15] Civalek, Ö. Vibration analysis of laminated composite conical shells by the method of discrete singular convolution based on the shear deformation theory. *Composites Part B: Engineering*, Vol. 45, No. 1, pp 1001-1009, 2013.
- [16] Wang, Q., Shao, D., Qin, B. A simple first-order shear deformation shell theory for vibration analysis of composite laminated open cylindrical shells with general boundary conditions. *Composite structures*, Vol. 184, pp. 211-232, 2018.
- [17] Guo, C., Liu, T., Bin, Q., Wang, Q., Wang, A. Free vibration analysis of coupled structures of laminated composite conical, cylindrical and spherical shells based on the spectral-Tchebychev technique. *Com*posite structures, Vol. 281, 114965, 2022.
- [18] Chen, X. L., Liu, G. R., Lim, S. P. An element free Galerkin method for the free vibration analysis of composite laminates of complicated shape. *Composite structures*, Vol. 59, No. 2, pp 279-289, 2003.
- [19] Ferreira, A. J. M., Carrera, E., Cinefra, M., Roque, C. M. C., Polit, O. Analysis of laminated shells by a sinusoidal shear deformation theory and radial basis functions collocation, accounting for through-the-thickness deformations. *Composites Part B: Engineering*, Vol. 42, No. 5, pp 1276-1284, 2011.
- [20] Liew, K. M., Zhao, X., Ferreira, A. J. M. A review of meshless methods for laminated and functionally graded plates and shells. *Composite structures*, Vol. 93, No. 8, pp 2031-2041, 2011.
- [21] Zuo, P., Shi, X., Ge, R., Luo, J., Ning, M. A new meshfree approach for vibration analysis of arbitrary restrained laminated composite cylindrical shell under thermal environment. *Engineering Analysis with Boundary Elements*, Vol. 140, pp 592-606, 2022.
- [22] Ilanko S, Monterrubio LE, Mochida Y. *The Rayleigh–Ritz Method for Structural Analysis*, John Wiley & Sons Ltd, 2014.
- [23] Qatu, M. S., Leissa, A. W. Free vibrations of completely free doubly curved laminated composite shallow shells. *Journal of Sound and Vibration*, Vol. 151, No. 1, pp 9-29, 1991.
- [24] Jin, G., Ye, T., Ma, X., Chen, Y., Su, Z., Xie, X. A unified approach for the vibration analysis of moderately thick composite laminated cylindrical shells with arbitrary boundary conditions. *International Journal of Mechanical Sciences*, Vol. 75, pp 357-376, 2013.
- [25] Li, H., Pang, F., Gao, C., Huo, R. A Jacobi-Ritz method for dynamic analysis of laminated composite shallow shells with general elastic restraints. *Composite Structures*, Vol. 242, 112091, 2020.
- [26] Zhang, Y., Shi, D. Vibration analysis of laminated composite coupled double cylindrical shell-annular-rectangular plate system. *Composite structures*, Vol. 281, 115020, 2022.
- [27] Zuo, P., Shi, X., Ge, R., Luo, J. Unified series solution for thermal vibration analysis of composite laminated joined conical-cylindrical shell with general boundary conditions. *Thin-Walled Structures*, 178, 109525, 2022.
- [28] Reddy JN. Mechanics of laminated composite plates and shells: theory and analysis. CRC press. 2003.
- [29] Milazzo A. Oliveri V., Post-buckling analysis of cracked multilayered composite plates by pb-2 Rayleigh–Ritz method, *Composite Structures*, Vol. 132, pp 75-86, 2015.
- [30] Benedetti I., Gulizzi V., Milazzo, A. X-Ritz Solution for Nonlinear Free Vibrations of Plates with Embedded Cracks. *Aerotecnica Missili e Spazio*, Vol. 98, No. 1, pp. 75-83, 2019.
- [31] Milazzo A. Free vibrations analysis of cracked variable stiffness composite plates by the eXtended Ritz method. *Mechanics of Advanced Materials and Structures*, Vol. 30, no. 8, pp 1675–1691, 2023.
- [32] Milazzo A, Guarino G, Gulizzi V. Buckling and post-buckling of variable stiffness plates with cutouts by a single-domain Ritz method. *Thin-Walled Structures*, Vol. 182, art. no. 110282, 2023. Vol. 30, No. 8, pp. 1675 1691, 2023.
- [33] Saye R I. High-Order Quadrature Methods for Implicitly Defined Surfaces and Volumes in Hyperrectangles. *SIAM Journal on Scientific Computing*, Vol. 37, No. 2, pp.A993-A1019,2015.
- [34] Gulizzi, V., Benedetti, I. and Milazzo. An implicit mesh discontinuous Galerkin formulation for higher-order plate theories, *Mechanics of Advanced Materials and Structures*, 27(17), 1494–1508, 2020
- [35] Gulizzi, V., Benedetti, I. and Milazzo, A. A high-resolution layer-wise discontinuous Galerkin formulation for multilayered composite plates, *Composite Structures*, 242, 112137,2020